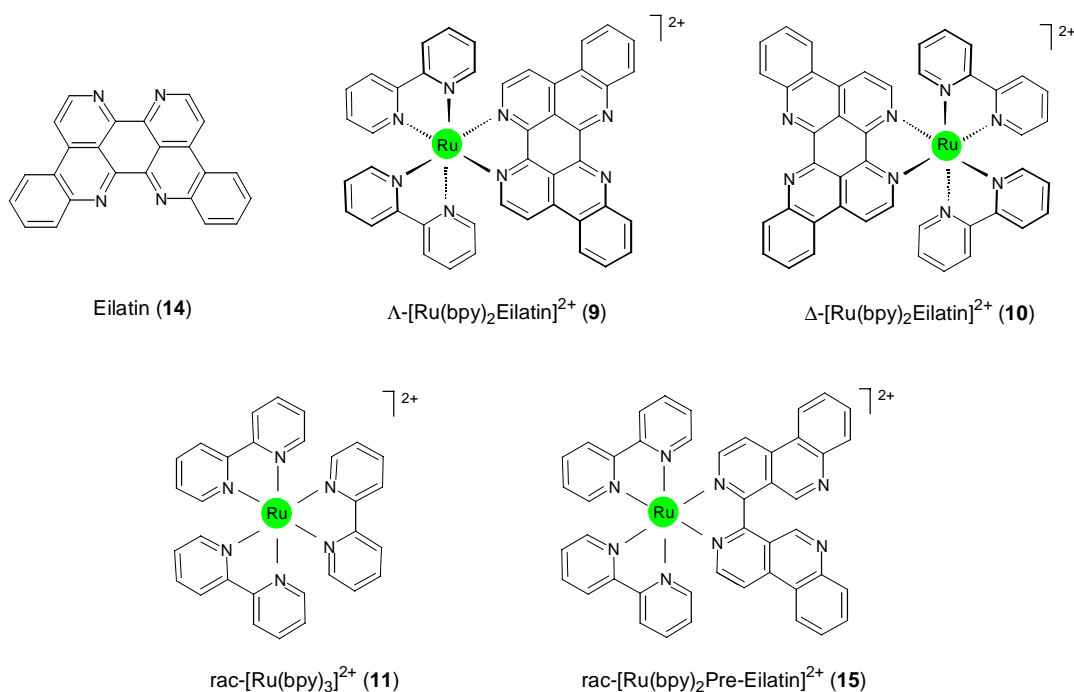
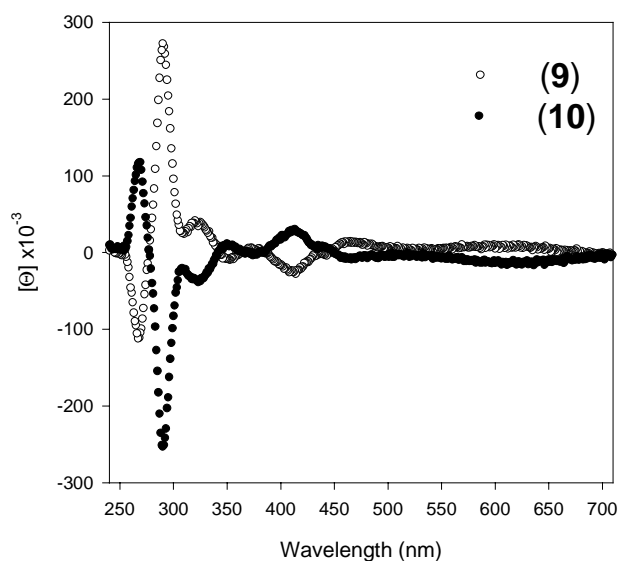


#### 4.0 New RRE Ligands: $[\text{Ru}(\text{bpy})_2\text{Eilatin}]^{2+}$

Eilatin (**14**) is a fused, heptacyclic aromatic alkaloid that was isolated from the Red Sea tunicate *Eudistoma sp.*<sup>101</sup> It is reported to possess cytotoxic and antiproliferation activities in a broad range of tissue cultures.<sup>102-104</sup> Eilatin is potentially a bi-facial metal chelator. Upon incorporation into octahedral metal complexes of the type  $[\text{Ru}(\text{L})_2\text{eilatin}]^{2+}$  (where L = bpy, phen, etc.), only the less hindered face of eilatin binds to the metal ion (Figure 4.0).<sup>105,106</sup> The enantiomerically pure metal complexes  $\Lambda$ - $[\text{Ru}(\text{bpy})_2\text{eilatin}]^{2+}$  (**9**) and  $\Delta$ - $[\text{Ru}(\text{bpy})_2\text{eilatin}]^{2+}$  (**10**) were synthesized from chiral precursors.<sup>106</sup> To confirm their correct assignment as  $\Lambda$  and  $\Delta$ , respectively, circular dichroism spectroscopy was employed (Figure 4.1).



**Figure 4.0:** Eilatin and eilatin-containing metal complexes. Unlike “free” eilatin (**14**), the chloride salts of **9**, **10**, **11**, and **15** are freely soluble in water. **15** is a synthetic pre-cursor of  $\text{rac-9/10}$  and provides an analog where the eilatin moiety is non-planar.<sup>107</sup>



**Figure 4.1:** CD spectra of the dichloride salts of  $\Lambda$ -[Ru(bpy)<sub>2</sub>eilatin]<sup>2+</sup> (**9**) and  $\Delta$ -[Ru(bpy)<sub>2</sub>eilatin]<sup>2+</sup> (**10**) in 50 mM sodium phosphate pH 7.5. See section E 4.0.1 for further experimental details. The dominant CD transitions (between 260 and 300 nm) for **9** and **10** match those predicted by the exciton theory for the correct assignment of the absolute configuration.<sup>108</sup>

$\Lambda$ -[Ru(bpy)<sub>2</sub>eilatin]<sup>2+</sup> (**9**) and  $\Delta$ -[Ru(bpy)<sub>2</sub>eilatin]<sup>2+</sup> (**10**) bind to the RRE with moderate affinity and high specificity (relative to a mixture of tRNAs, see Section 3.2 and reference 81). Fluorescence anisotropy, native gel-shift electrophoresis, and the solid-phase binding assay all indicate that **9** and **10** bind to the RRE and displace a Rev protein fragment with approximately 10-times greater activities as compared to the widely studied RNA ligand neomycin B (Section 3.2 – 3.3). The ability of **9** and **10** to inhibit Rev-RRE binding implicated their potential use as anti-HIV agents. To explore this possibility, the anti-HIV activities of **9**, **10**, **11**, and **15** were measured in cell cultures, using HIV-1 infected CD4+ HeLa cells. The dose-dependent decrease in plaques (syncytia) is shown in Figure 4.2 and IC<sub>50</sub> values are summarized in Table 4.1. Plaques are multinucleated cellular

masses that are initiated by HIV-infected cells due to the surface expression of the ENV protein, which allows CD4+ cells to fuse with infected cells, resulting in large multinucleated cell masses. Plaque formation may be the primary cause of T-cell death *in vivo*.<sup>109</sup>

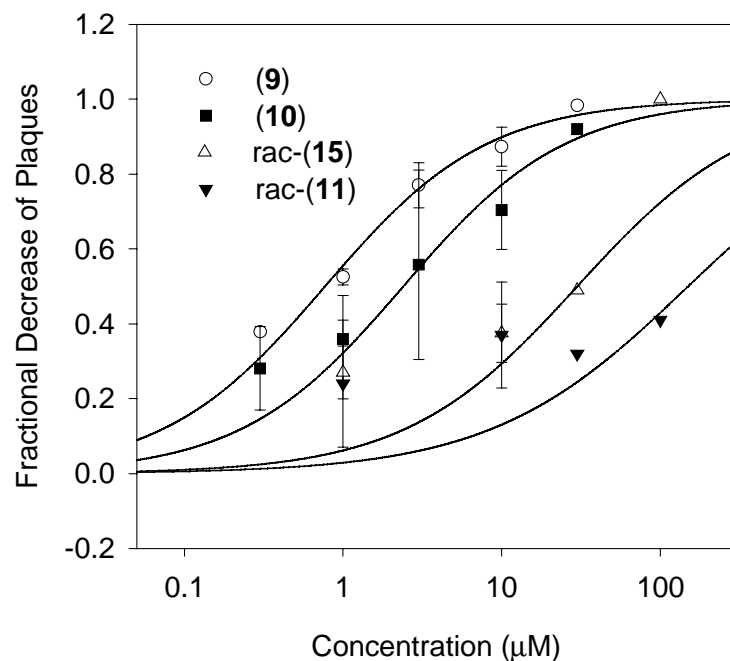


**Figure 4.2:** The anti-HIV activity of compounds **9**, **10**, **11**, and **15** as evidenced by the fractional decrease in plaque formation in CD4+ HeLa cells. Assays were conducted at the Center for AIDS Research, San Diego. See experimental section E 4.0.2 and reference 110 for details. Free eilatin (**14**) was not evaluated for anti-HIV activity due to its poor solubility in DMSO/water and its high toxicity to cell cultures. **9** was also evaluated for anti-HIV activity in human peripheral blood monocytes (PBMC) by measuring the dose-dependent decrease in HIV-1 p24 expression using ELISA (as described in E 4.0.3 and reference 110); this assay also yielded an  $IC_{50} = 1 \mu\text{M}$ .

Compounds **9** and **10** have anti-HIV activities that are from 15 to over 100-fold greater than those of **11** and **15**. This clearly illustrates the significance of the eilatin moiety to the anti-HIV activities of **9** and **10**. To date, only one other family

of polypyridine-containing metal complexes has been shown to inhibit HIV replication.<sup>111</sup> These compounds, however, are chemically reactive, create covalent cross-links to DNA, and are highly toxic.<sup>111a</sup> In contrast, compounds **9** and **10** are chemically inert, and show no sign of toxicity to HeLa cells (through 100  $\mu\text{M}$ ).

**Table 4.1:** IC<sub>50</sub> values ( $\mu\text{M}$ ) for HIV inhibition and for RevFI displacement experiments from RRE66 and TAR31 (determined by fluorescence anisotropy).

Compound	HIV-1 <sup>a</sup>	RRE66 <sup>b</sup>	TAR31 <sup>b</sup>
<b>9</b>	0.8	0.9	5.3
<b>10</b>	2.0	1.1	3.5
rac- <b>9/10</b>	0.9	1.0	3.9
rac- <b>15</b>	30	20	30
rac- <b>11</b>	>100	>170 <sup>c</sup>	>86 <sup>c</sup>

<sup>a</sup> Concentration needed to decrease HIV-1 activity by 50% in HeLa plaque assay, standard deviation is less than  $\pm 40\%$  of reported value.

<sup>b</sup> Concentration needed to displace 50% of RevFI from 100 nM of each RNA construct, standard deviation is less than  $\pm 20\%$  of reported value.

<sup>c</sup> Only limits can be determined with this method due to fluorescence interference from Ru(bpy)<sub>3</sub>.

To investigate the ability of **9**, **10**, **11**, and **15** to interfere with the function of the RRE66 and the TAR31, fluorescence anisotropy (Section 3.1) was used to monitor the ability of each compound to displace RevFI from each RNA. A summary of RevFI displacement data is given in Table 4.1. Overall, a correlation exists between the anti-HIV activity of each compound and its affinity for HIV RNA. Compared to **9** and **10**, the non-planar analog [Ru(bpy)<sub>2</sub>pre-eilatin]<sup>2+</sup> (**15**) has approximately a 20-fold lower RNA affinity and lower anti-HIV activity (Table

4.1). The poor nucleic acid affinity of  $[\text{Ru}(\text{bpy})_3]^{2+}$  (**11**) appears to be a general phenomenon.<sup>112</sup> Gel shift electrophoresis confirms that  $[\text{Ru}(\text{bpy})_3]^{2+}$  shows no inhibition of the Rev-RRE complex through 10 mM (Figure 3.9). This indicates that complementary electrostatic interactions are not the primary energetic driving force for the binding of eilatin-containing metal complexes (**9** and **10**) to the RRE. The poor anti-HIV activities and poor HIV RNA affinities of **11** and **14** support a correlation between the nucleic acid affinity and anti-HIV activity of these octahedral metal complexes (Table 4.1). There are, of course, other potential mechanisms that explain the anti-HIV activities of **9** and **10**. In conjunction with Immusol Inc. (Sorrento Valley, CA) the mechanism(s) that govern the anti-HIV activities of **9** and **10** are currently being examined *in vivo*.

Preferential binding of both **9** and **10** to the RRE66 as compared to the TAR31, is suggested by the 3-5 fold lower  $\text{IC}_{50}$  values observed for RevFI peptide displacement for RRE66 versus TAR31 (Table 4.1). Compared to TAR31, the RRE66 has a higher affinity to RevFI (Table 3.0), so it should be “more difficult” to displace RevFI from the RRE66 than TAR31. Differences in the binding stoichiometries could, in principle, make the trends in  $\text{IC}_{50}$  values inconsistent with the trends in affinity ( $K_d$ ). Direct binding studies have been utilized to confirm the higher affinity of **9** and **10** for the RRE versus TAR (presented later).

To confirm the trends indicated by peptide displacement and to expand the study to include simple duplex RNAs and DNAs, ethidium bromide displacement

assays were conducted using the RRE66, TAR31, and 6 other nucleic acids (see Section 3.3 and Figure 3.12 for examples of ethidium displacement experiments using **9**, **10**, and **15**). Table 4.2 summarizes the IC<sub>50</sub> values for ethidium displacement from the RRE66, TAR31, poly r[I] – poly r[C], poly r[A] – poly r[U], calf thymus (C.T.) DNA, poly d[AT] – poly d[AT], and poly d[GC] – poly d[GC]. Since ethidium has variable binding stoichiometries and a broad range of affinities to different nucleic acids, the IC<sub>50</sub> values in Table 4.2 are not directly comparable between different nucleic acids. Rather a comparison of each compound for each nucleic acid is more appropriate (comparisons should be made vertically, not horizontally).

**Table 4.2:** IC<sub>50</sub> values (μM) for ethidium displacement.<sup>a</sup> See E 3.3 for experimental details.

Compound	RRE66 <sup>b</sup>	TAR31 <sup>b</sup>	poly r[I] - poly r[C] <sup>c</sup>	Poly r[I] - poly r[C] <sup>d</sup>	poly r[A]- poly r[U] <sup>d</sup>	C.T. DNA <sup>d</sup>	poly d[AT] <sup>d</sup>	poly d[GC] <sup>d</sup>
<b>9</b>	0.25	1.8	10.5	1.5	2.0	0.1	0.07	0.25
<b>10</b>	0.4	1.6	7.7	1.4	5.0	0.4	0.2	0.4
rac- <b>15</b>	10	9.0	22	4.0	23	7.0	n.d. <sup>e</sup>	n.d. <sup>e</sup>

<sup>a</sup> Errors associated with measurement within ± 25% of reported value.

<sup>b</sup> IC<sub>50</sub> values measured using 50 nM of RNA construct.

<sup>c</sup> IC<sub>50</sub> values measured using 11 μM of duplex base pairs.

<sup>d</sup> IC<sub>50</sub> values measured using 0.88 μM of duplex base pairs.

<sup>e</sup> Not determined.

Consistent with RevFI displacement experiments, ethidium displacement suggests that the RRE66 has a small preferential binding of **9** over **10**, while the TAR31 has a slight preference for the other enantiomer (Table 4.2). Simple duplex RNAs also exhibit variable selectivity between **9** and **10**. Poly r[A] – poly r[U] shows better binding of **9** over **10**, while poly r[I] – poly r[C] shows a small,

yet consistent, selectivity for **10** over **9**. To our knowledge these are the first reported examples of octahedral metal complexes that exhibit variable chiral discrimination between simple duplex RNAs. Consistent with conclusions from the solid-phase assay (Section 3.2), all three of the simple duplex DNAs exhibit preferential binding of **9** over **10** (Table 4.2). Interestingly, this is the opposite enantiomeric selectivity as reported for most other metal complex-DNA interactions to date.<sup>115a-e</sup>

Ethidium displacement experiments indicate that, in general, **9** and **10** have higher affinity to all nucleic acids as compared to **15**. The absence of a single carbon-carbon bond in  $[\text{Ru}(\text{bpy})_2\text{pre-eilatin}]^{2+}$  (**15**) should impart a fluctuating dihedral twist averaging  $25^\circ$  between the two tricyclic ring systems in the pre-eilatin ligand.<sup>113</sup> Prior to these studies, it was unknown how this twisting would affect nucleic acid affinity.<sup>114</sup> A crystal structure of rac-(**9/10**) shows the RMS deviation of eilatin from planarity (including hydrogen atoms) is  $0.130 \text{ \AA}$ .<sup>106</sup> Without hydrogen atoms, the RMS deviation from planarity is  $0.098 \text{ \AA}$ .<sup>106</sup> The deviation of eilatin itself (**14**) from planarity is  $0.044 \text{ \AA}$  (without H's).<sup>101</sup> Eilatin is, therefore, nearly a planar ligand. These studies indicate that the planarity of the eilatin ligand is necessary for the anti-HIV activities and the nucleic acid binding exhibited by **9** and **10**.

Octahedral metal complexes can bind to nucleic acids through various modes, including: intercalation, electrostatic, and groove binding.<sup>115a-k</sup> Given the apparent “planarity requirement” for the high-affinity binding of **9** and **10** to nucleic acids, we investigated the possibility that **9** and **10** bind by intercalation. The viscosity of a DNA solution was measured with increasing concentrations of rac- **9/10** (Figure 4.3). In accordance with the hypothesis proposed by Lerman,<sup>116</sup> the viscosity of a DNA solution increases upon the addition of an intercalating agent.<sup>117</sup> Upon intercalation of a small molecule, the axial length of DNA increases and it becomes more rigid. Both factors increase the frictional coefficient, and hence, the viscosity of the DNA in solution.<sup>117</sup>

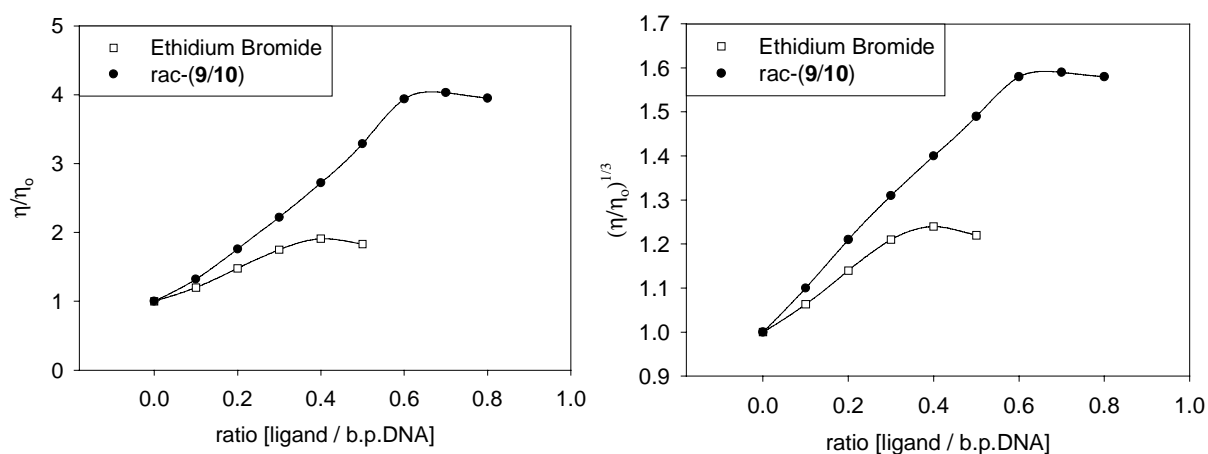


**Figure 4.3:** Changes in the viscosity of a solution of calf thymus DNA (500  $\mu\text{M}$  b.p.) with increasing concentrations of ligand. The viscosity of a DNA solution is determined by measuring the time needed for it to flow through a capillary viscometer.  $\eta$  is the viscosity of the solution in the presence of a ligand,  $\eta_0$  is the viscosity of the DNA-only solution. Random errors for this experiment are approximately the size of the symbols used for each point. A low-salt buffer (50 mM sodium phosphate pH 7.5) was used. See Section E 4.0.4 for additional experimental details.

Since the change in viscosity should be proportional to the change in the axial length of a rigid DNA molecule to the third power, viscosity results are often reported as  $(\eta/\eta_0)^{1/3}$  versus molar fraction of the ligand (Figure 4.3 Right).<sup>117</sup> Theory predicts that for an “ideal” intercalating agent, this plot will be linear with a slope of 1.0.<sup>117</sup> Interestingly, rac-(**9/10**) has a slope of 1.0 and ethidium has a slope of 0.7. Other groups have also observed a slope of less than 1.0 for ethidium.<sup>115i</sup> At low ionic strengths, ethidium can bind to DNA by both intercalation and by surface-binding via electrostatic interactions.<sup>86</sup> Compounds that bind to duplexes through electrostatic interactions, such as tobramycin (**3**), can decrease the viscosity of the nucleic acid solution.<sup>118</sup> This may explain why, under these conditions, viscometric analysis of the ethidium-DNA complex yields a slope significantly lower than 1.0 (Figure 4.3 Right).

Other interesting differences between rac-**9/10** versus ethidium (**12**) are also apparent in the viscosity titrations (Figure 4.3). The ratio at which the DNA becomes saturated is significantly different for each compound. The curve for ethidium reaches saturation at ~3 ethidium molecules / 10 base pairs. This value is consistent with the reported binding stoichiometry of ethidium to C.T. DNA.<sup>87</sup> This is also the same binding stoichiometry reported by Chaires for  $[\text{Ru}(\text{phen})_2\text{DPPZ}]^{2+}$  (a metal complex very similar to **9** and **10**).<sup>115c</sup> For rac-**9/10**, however, saturation is reached at much higher ratios (Figure 4.5), suggesting a maximum binding stoichiometry of ~ 6 equivalents of ligand for every 10 base-pairs of DNA. This is an unusually high binding stoichiometry for such a large

metal complex! Only one other example of such a high binding stoichiometry for a metal complex is found in the literature.<sup>119</sup> Barton and Lippard report ~6.7 equivalents of [(terpy)Pt(HET)]<sup>1+</sup> per every 10 base-pairs of poly r(A) – poly r(U).<sup>119</sup> This metal complex is, however, square planar, and the intercalation of this compound into duplexes should be much less sterically hindered as compared to **9** and **10**.

To better examine the nucleic acid sequence and structure specificity of **9** and **10**, direct binding studies have been conducted by monitoring the UV absorbance spectrum of either **9** or **10** as a function of nucleic acid concentration (Figure 4.4). Compounds **9** and **10** exhibit multiple electronic transitions in their absorbance spectra that are sensitive to nucleic acid binding. The presence of multiple isosbestic points, and saturation at high DNA concentrations, suggests a simple two-state transition exists between the “bound” versus “free” states of the ligand upon titration of nucleic acid (Figure 4.4). The concentration of nucleic acid needed to bind ½ of each compound (defined as the C<sub>50</sub> value) is determined by assuming a linear relationship between the spectral changes and the fraction of ligand bound. A lower C<sub>50</sub> value suggests a higher binding affinity and/or more binding sites.

Titration were conducted using many different nucleic acids by observing the UV-vis absorption changes of either **9**, **10**, or **12** as a function of nucleic acid concentration (Table 4.3). For all duplex nucleic acids tested, the UV-vis

absorbance spectra of **9** and **10** show changes similar to those observed upon titration of Calf Thymus (CT) DNA (Figure 4.4). The absolute change in intensity and degree of red-shifting are slightly different for each nucleic acid tested, but all titrations exhibit simple two state transitions (see section E 4.0.5 for the “raw” spectral data of **9** and **10** upon titration of each nucleic acid). Each nucleic acid endows unique spectral changes to **9** and **10**, but no obvious correlation is found between the composition of the nucleic acid and the spectral changes exhibited by ligand (see section E 4.0.5).

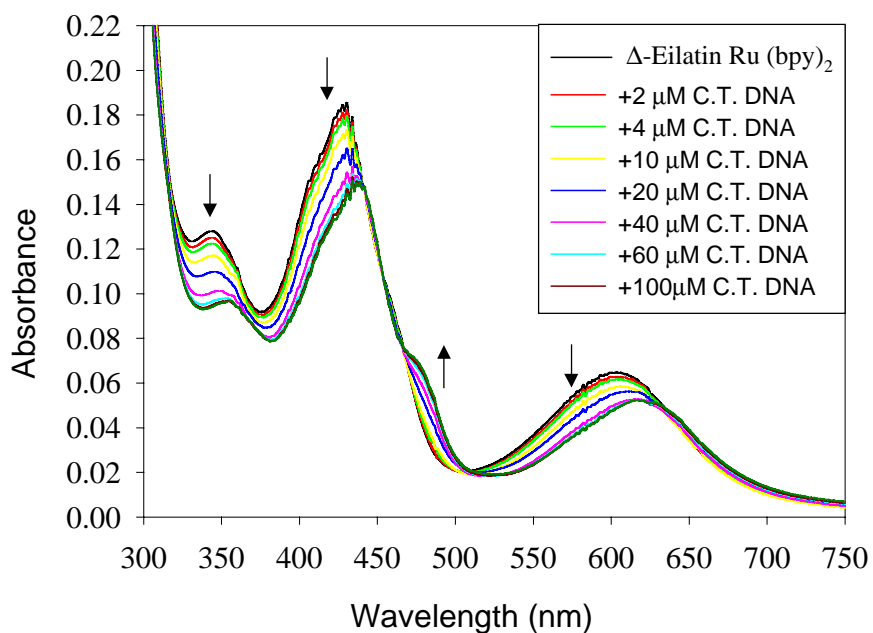


**Figure 4.4:** Uv-vis absorbance spectrum of **10** ( $8 \mu\text{M}$ ) as a function of calf thymus DNA (concentration in base-pairs). See E 4.0.5 for additional experimental details and the raw data for all polymeric nucleic acids tested.

Consistent with the results from the solid-phase assay (Section 3.3), thermal denaturation (Section 3.5), and ethidium bromide displacement experiments (Table 4.2), the direct titration experiments indicate that **9** has a higher affinity for CT DNA as compared to **10** (Table 4.3). Interestingly, both **9** and **10** exhibit

sequence selectivity in the binding double-stranded DNA and RNA. For example, **10** has over a 5-fold higher affinity for poly d(G) – d(C) as compared to poly d(GC) – d(GC), and both **9** and **10** have a higher affinity to poly d(AT) – d(AT) as compared to poly d(A) – d(T) (Table 4.3).

The classic intercalating agent ethidium bromide (**12**) has been evaluated for nucleic acid selectivity by monitoring its changes in UV-vis absorption spectrum, and the eilatin “free ligand” (**14**) has been evaluated using fluorescence emission spectroscopy (presented below). All four compounds have a much higher affinity to poly r(A) – r(U) as compared to both poly r(I) – r(C), and r(G) – r(C). This may indicate that some duplex nucleic acids have, in general, a low affinity for “any” intercalating agent. Some nucleic acids, on the other hand, are highly sensitive to the identity of the intercalating agent. For example, poly d(A) – d(T), has a very low affinity for ethidium (**12**), a modest affinity for the metal complexes (**9** and **10**), and a very high affinity for the free eilatin ligand (**14**) (Table 4.3) All four compounds exhibit a moderate selectivity for duplex DNA over duplex RNA. Each compound, for example, has approximately a 10-fold higher affinity for poly d(G) – d(C) versus poly r(G) – r(C) (Table 4.3). We conclude that, for the most part, the trends in the nucleic acid affinity for **9**, **10**, and **12** are similar for all the *duplex* nucleic acids tested. We interpret this as additional evidence that **9** and **10** bind to duplex nucleic acids via intercalation.

**Table 4.3:**  $C_{50}$  values ( $\mu\text{M}$ )\* for  $8\ \mu\text{M}$  of  $\Lambda\text{-}[\text{Ru}(\text{bpy})_2\text{eilatin}]^{2+}$  (**9**),  $8\ \mu\text{M}$   $\Delta\text{-}[\text{Ru}(\text{bpy})_2\text{eilatin}]^{2+}$  (**10**),  $8\ \mu\text{M}$  ethidium bromide (**12**), and  $0.1\ \mu\text{M}$  eilatin (**14**).

Nucleic Acid	$\Lambda\text{-}[\text{Ru}(\text{bpy})_2\text{eilatin}]^{2+}$ ( <b>9</b> )	$\Delta\text{-}[\text{Ru}(\text{bpy})_2\text{eilatin}]^{2+}$ ( <b>10</b> )	ethidium bromide ( <b>12</b> )**	eilatin ( <b>14</b> )***
C.T. DNA	18	27	20	3
Poly d(A) – Poly d(T)	13	23	105	1
Poly d(AT) – Poly d(AT)	9	8	13	5
Poly d(G) – Poly d(C)	15	13	22	5
Poly d(GC) – Poly d(GC)	18	55	16	8
Poly r(A) – Poly r(U)	13	22	18	12
Poly r(G) – Poly r(C)	125	85	400	20
Poly r(I) – Poly r(C)	200	180	170	150
Poly r(U)	8	8	4000	>2000
Poly r(C)	52	75	8000	>1000
Poly r(A)	14	13	1500	70
Poly r(G)	18	20	240	4
Poly r(I)	13	10	950	0.2
Oligo r(I) <sub>15</sub>	68	53	n.d.	n.d.
Poly d(A)	20	~200	n.d.	n.d.
Oligo d(A) <sub>15</sub>	~200	70	n.d.	n.d.
Oligo d(T) <sub>15</sub>	21	21	n.d.	n.d.

\*  $C_{50}$  values for duplexes are reported per base pair, the values for single-stranded polymers are reported per base. The approximate experimental deviation for all values is less than or equal to  $\pm 35\%$  of the reported  $C_{50}$  value.

\*\* Changes in UV-vis absorption monitored for duplex nucleic acids, and changes in emission monitored for single-stranded nucleic acids.

\*\*\* Compared to **9**, **10**, **12**, a much lower concentration of **14** was used for spectroscopic measurements ( $8.0\ \mu\text{M}$  versus  $0.1\ \mu\text{M}$ , respectively), the  $C_{50}$  values for **14**, cannot, therefore, be directly compared to those of **9**, **10**, and **12**.

The eilatin-containing metal complexes **9** and **10** do, however, demonstrate some interesting differences when compared to ethidium bromide (**12**); the most surprising revelation is their high affinity for single-stranded nucleic acids (Table 4.3). Classic intercalating agents, like ethidium bromide, exhibit a relatively low affinity for single-stranded RNAs and DNAs. Ethidium has a 1,000-fold lower affinity for most single-stranded nucleic acids as compared to duplex nucleic acids (Table 4.3). **9** and **10**, however, exhibit a higher apparent affinity for both poly r(U), and poly r(I) as compared to most duplex nucleic acids. In terms of RNA selectivity, **9** and **10** have a higher apparent affinity for the single-stranded versus double-stranded polymeric RNA. Since most natural RNAs, including the RRE, have bulged regions and other features with single-strand characteristics, it is possible that the single-stranded regions bind, with high affinity, to **9** and **10**. Differences in binding stoichiometry could, however, make the  $C_{50}$  values in Table 4.3 disproportionate to the actual affinities ( $K_d$ ). To determine the single stranded binding stoichiometries of **9** and **10**, the UV-vis absorbance spectrum of a high concentration of **10** (40  $\mu$ M) was monitored upon titration poly r(U) (Figure 4.5). Interestingly, a very high stoichiometry is indicated, where approximately 5 equivalents of **9** or **10** are bound per every 10 bases of poly r(U). This is very similar to the stoichiometry observed for CT DNA, where 6 equivalents of rac-**9/10** bind for every 10 base pairs (Figure 4.5). Another duplex DNA, poly d(AT) – poly d(AT), also exhibits the same binding stoichiometry for both **9** and **10** (at 5 equivalents per every 10 base pairs) (not shown).

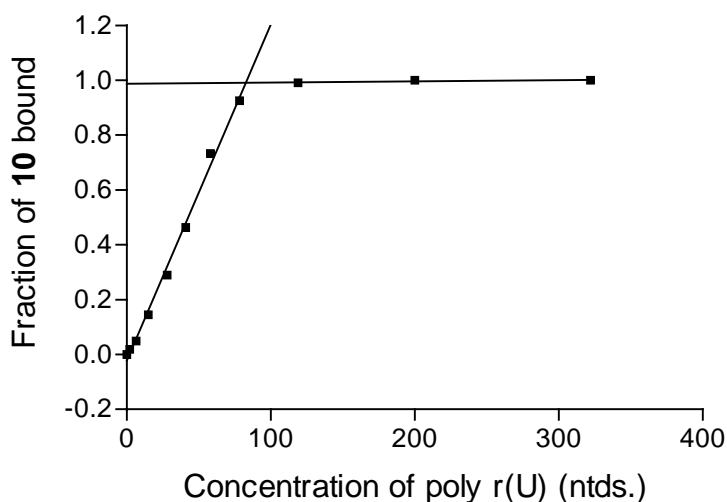


**Figure 4.5:** At high concentrations of **10** ( $40\ \mu\text{M}$ ), the binding isotherm for poly r(U) is composed of two linear elements, the intersection of these lines (at  $80\ \mu\text{M}$  of poly r(U)) indicates the maximum binding stoichiometry for **10** is 1 equivalent for every 2 bases of poly r(U). The other enantiomer **9** yields the same result. The same experiment was conducted with duplex DNA and also yielded a binding stoichiometry of 1 equivalent of either **9** or **10** for every 2 base pairs of poly d(AT) – d(AT).

Titration using poly r(U) were also conducted with either  $4\ \mu\text{M}$  or  $8\ \mu\text{M}$  of **10** (Figure 4.6). At  $4\ \mu\text{M}$  and  $8\ \mu\text{M}$  of **10**, the binding data fit very well to Hill coefficients of  $n=2$  (Figure 4.6). This suggests positive cooperativity for these binding interactions (Section 3.6). Duplex nucleic acids can also show positive cooperativity in their binding of **9** and **10**. For example, both poly d(AT) – d(AT) and poly d(A) – d(T) have Hill coefficients of  $n = 2$  for binding to both **9** and **10**. Indeed, all of the “higher affinity” interactions ( $C_{50} < 30\ \mu\text{M}$ , Table 4.3) show some degree of positive cooperativity in their binding of **9** and **10** (Hill coefficients range from 1.5 to 2.2).

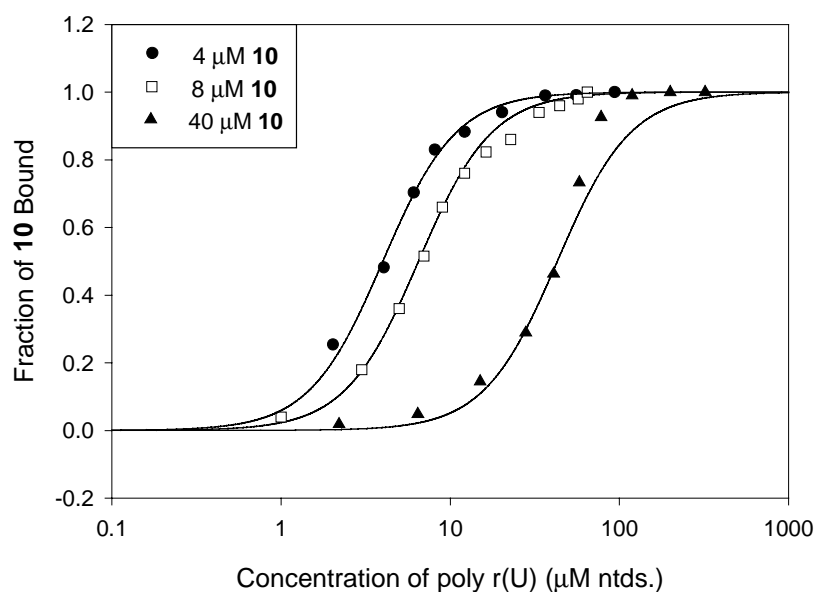


**Figure 4.6:** Association of poly r(U) with **10** at three different concentrations. At 4  $\mu\text{M}$  and 8  $\mu\text{M}$  a good fit is found for a Hill coefficient of  $n = 2$ . As expected, a poor fit is found at 40  $\mu\text{M}$ .

To further investigate the high affinity and cooperative binding of **9** and **10** to single-stranded poly r(U), thermal denaturation experiments were conducted (Figure 4.7). By themselves, the UV adsorption of **9**, **10**, and poly r(U) (260 nm) show only small non-cooperative changes as a function of temperature (Figure 4.7). The complex formed between **10** and poly r(U), however, shows a highly cooperative melting behavior reminiscent of duplex denaturation (Figure 4.7 solid line). The complex formed between **9** and poly r(U), however, shows multiple, non-reversible transitions (Figure 4.7 dotted line). It is possible that under these conditions, some non-specific aggregation between **9** and poly r(U) occurs. The complex between **10** and poly r(U), however, appears well-behaved (Figure 4.7).

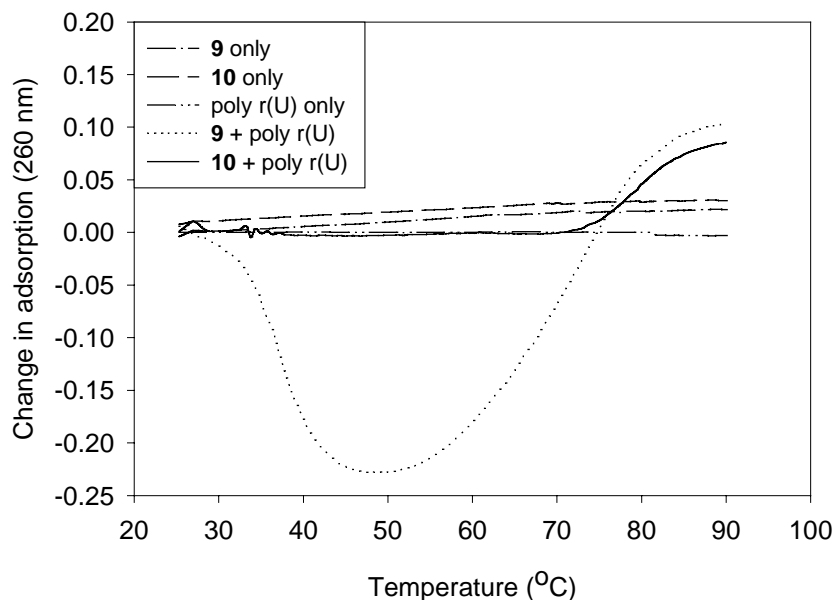


**Figure 4.7:** Change in adsorption of poly r(U) (30  $\mu$ M of bases) with or without, **9** or **10** (15  $\mu$ M). See section E 4.0.6 for experimental details.

The thermodynamic parameters of the melting transition (70 – 90 °C) for the poly r(U)-**10** complex can be fit to a van't Hoff plot (Figure 4.8). This analysis assumes that the melting of the complex represents a simple two-state transition. Based upon their known binding stoichiometry (Figure 4.5), a 2:1 ratio of poly r(U) bases to **10** was used for the  $T_m$  experiment so that excess ligand would not drive complex formation. From the van't Hoff plot (Figure 4.8), a large enthalpy of formation ( $\Delta H^0 = -84$  kcal / mole) and a modest entropy of formation ( $\Delta S^0 = -240$  cal / mole  $K^{-1}$ ) are calculated. These values represent the energetic parameters for the complex as a whole and do not reflect the binding of individual molecules of **10** to poly r(U). These  $\Delta H^0$  to  $\Delta S^0$  values are similar to those for the melting of

long polymeric nucleic acids. For example, CT DNA, under these same conditions has enthalpy of formation ( $\Delta H^0 = -82$  kcal / mole) and an entropy of formation ( $\Delta S^0 = -280$  kcal / mole  $K^{-1}$ ) (data not shown). Compared to the poly r(U)-**10** complex and to CT DNA, shorter duplex nucleic acids have smaller  $\Delta S^0$  terms and, therefore, exhibit less cooperative melting transitions.<sup>120</sup>

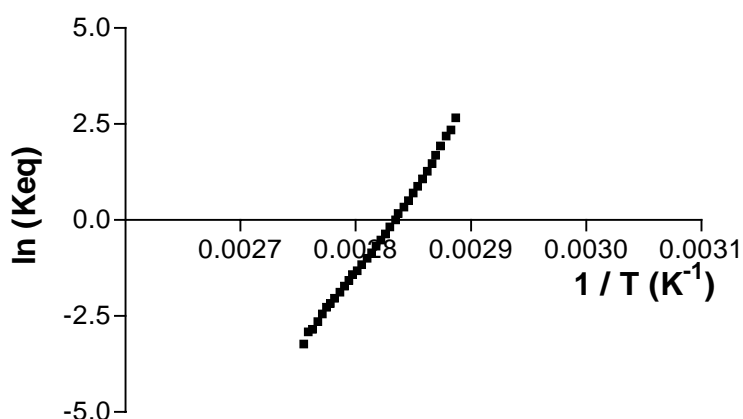


**Figure 4.8:** van't Hoff plot of the thermal melting of the poly r(U)-**10** complex.  $K_{eq}$  is taken as the fraction of folded complex relative to unfolded complex.  $\Delta H^0 = - (R \cdot \text{slope})$  and  $\Delta S^0 = \Delta H^0 / T_m$  ( $^{\circ}K$ ).

The melting transition of the poly r(U)-**10** complex provides additional evidence that the binding interaction between **10** and poly r(U) is highly cooperative and large binding energies ( $\Delta G_{\text{complex}} = 8 - 12$  kcal / mole) are involved. This raises the possibility that the poly r(U)-**10** complex is a well-ordered supermolecular structure suitable for crystallization and subsequent analysis by X-ray crystallography.

Interestingly, the non-polymeric nucleic acids (RRE JW, TAR 31, and tRNA<sup>Phe</sup>) do *not* show cooperativity in their binding of **9** and **10** (Hill coefficients range from 1.1 – 1.4). Scatchard plots can, therefore, be used to establish the average affinity and stoichiometry of **9** and **10** for binding these RNA transcripts (Figure 4.9 and Table 4.4).

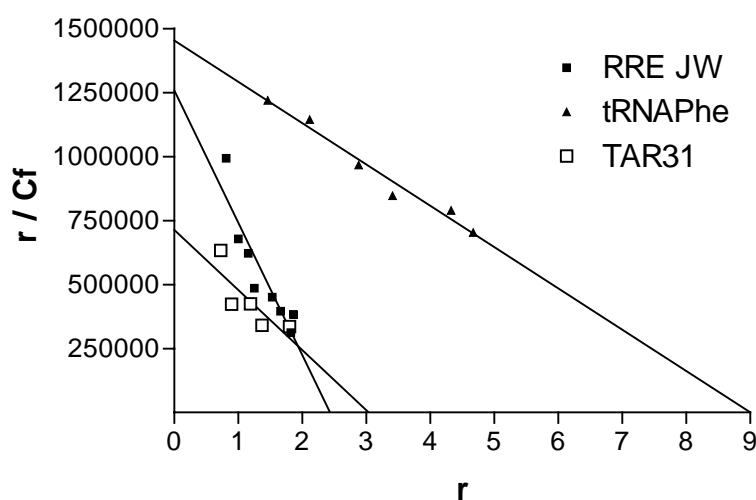


**Figure 4.9:** Scatchard analysis of the interaction between **9** and the RRE JW, tRNA<sup>Phe</sup>, and TAR31. The slope of the graph =  $1/K_d(\text{ave})$ , and the  $r$  value at  $r / C_f = 0$  is the number of apparent binding sites.

**Table 4.4:** Summary of the binding stoichiometries and average affinity of **9** and **10** for RRE JW, tRNA<sup>Phe</sup> and TAR 31.

Nucleic Acid	Binding sites for <b>9</b>	Average $K_d$ ( $\mu\text{M}$ ) for <b>9</b>	Binding sites for <b>10</b>	Average $K_d$ ( $\mu\text{M}$ ) for <b>10</b>
RRE JW	2.4	1.9	3.8	1
tRNA <sup>Phe</sup>	9	5.6	10	5.6
TAR 31	3	4.6	4	9

Non-whole numbers for the binding stoichiometry are obtained for some of the interactions (Table 4.4). This suggests that some RNAs have multiple, nonequivalent binding sites, and therefore, the reported affinity ( $K_d$ ) represents

the average affinity to all of the “active” binding sites. Consistent with the Rev peptide and ethidium displacement experiments as well as the solid-phase assay, **9** and **10** have a higher affinity for the RRE as compared to both TAR31 and tRNA<sup>Phe</sup>. Unfortunately, due to the limited sensitivity of monitoring changes in UV-vis absorption, it is difficult to probe the highest affinity binding site(s) on the RRE. Since **9** and **10** are non-emissive, low  $\mu\text{M}$  concentrations are needed to observe the spectral changes of these compounds. For example, even if the RRE possesses a 10 nM binding site, it cannot be characterized under these conditions since the metal complex is at a much higher concentration compared to the affinity. This limitation is also reflected in some of the  $C_{50}$  values reported in Table 4.3. Since the concentration of **9** and **10** used for these titrations is 8  $\mu\text{M}$ , and the binding stoichiometry is approximately 1 ligand per every 2 bases (or every 2 base-pairs), the theoretical minimum  $C_{50}$  value for all polymeric nucleic acids is 8  $\mu\text{M}$  (Table 4.3). We can only report, therefore, that the interaction between poly r(U) and both **9** and **10** exhibit affinities of  $K_d < 0.5 \mu\text{M}$  (Table 4.5).

Given the unusual nucleic acid selectivities of **9** and **10**, we decided to investigate the nucleic acid affinity and specificity of “free” eilatin (**14**). Unlike the eilatin-containing metal complexes (**9** and **10**), eilatin itself (**14**) is highly emissive and shows changes in its emission spectrum upon addition of nucleic acids (Figure 4.11). For all nucleic acids tested, a decrease in emission intensity is observed, allowing for  $C_{50}$  values to be established (Figure 4.10 and Table 4.3).

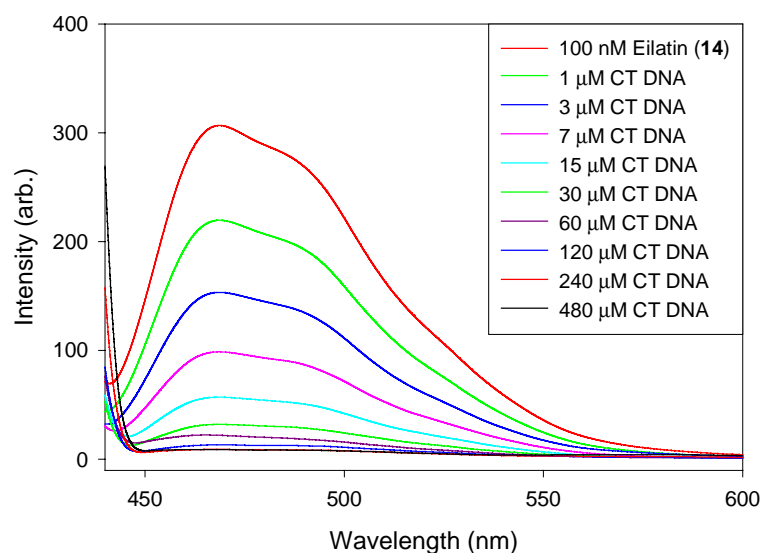


**Figure 4.10:** Changes in the fluorescence emission spectrum of 0.1  $\mu\text{M}$  eilatin (**14**) upon addition of CT DNA. Nearly identical changes are seen for all other nucleic acids tested. Excitation is at 417 nm, see Section E 4.0.7 for additional experimental details.

The  $C_{50}$  values measured for eilatin (**14**) are not directly comparable with those determined for **9**, **10**, and **12** (Table 4.3). Due to detection limits of **9** and **10**, and the limited water solubility of **14**, the concentration of eilatin (**14**) used for the fluorescence experiments is 80-fold lower than the concentrations needed for the UV-vis titrations of **9**, **10**, and **12** (Table 4.3). Binding constants for all of the compounds can be estimated from the  $C_{50}$  values (summarized in Table 4.5). For eilatin (**14**), the  $K_d \approx (C_{50} / 2) - 0.05$  (this assumes that binding is non-cooperative and that the neighbor exclusion limit of **14** is one molecule per 2 base pairs).  $K_d$  values have also been estimated for the eilatin-containing metal complexes (**9** and **10**), and for ethidium bromide (**12**) (Table 4.5). All estimates are equal to the  $C_{50}$  value divided by the binding stoichiometry, minus half the concentration of the ligand. Issues related to the cooperative binding of **9** and **10** do, however,

complicate this estimate. Nonetheless, these  $K_d$  estimates allow for a more direct comparison of the binding affinities of all four compounds (Table 4.5).

Unlike the eilatin-containing metal complexes (**9** and **10**), eilatin (**14**) is *not* very soluble in water (maximum concentration of **14** at pH 7.5 = 3  $\mu\text{M}$ ). Limited water solubility prevents Rev peptide and ethidium displacement experiments from reaching saturation. The  $\text{IC}_{50}$  value of **14** for Rev-RRE inhibition, for example, is  $>3 \mu\text{M}$  (Figure 4.11). This represents, however, at least a 3-fold lower Rev-RRE inhibition activity as compared to **9** and **10**. Eilatin (**14**) does, however, bind to the RRE with high affinity (Figure 4.11). Fluorescence binding studies indicate that eilatin (**14**) binds to one or more sites on the RREJW with a  $K_d$  of approximately 0.5  $\mu\text{M}$ , but cannot displace Rev by binding to these site(s).

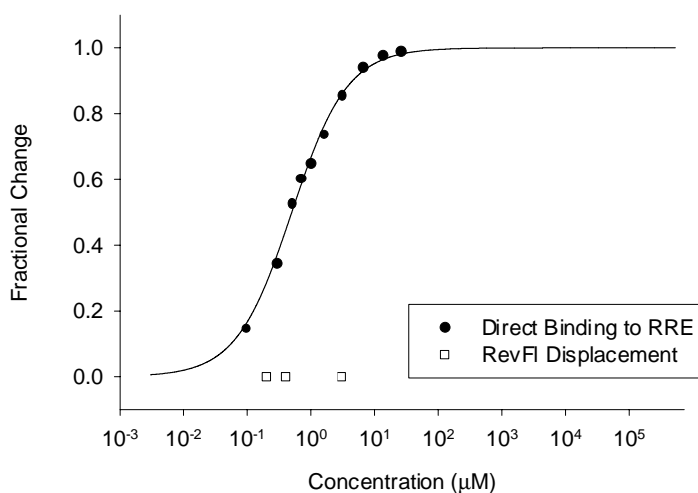


**Figure 4.11:** A comparisons between the “direct” binding of eilatin (**14**) to the RRE JW and its ability to inhibit Rev-RRE66 binding. For the direct binding experiment, the fluorescence intensity of eilatin was monitored as a function of RRE JW concentration. The direct binding data is fit to a  $C_{50}$  value of 0.5  $\mu\text{M}$  with no cooperativity (Hill coefficient = 1.0). For the RevFI displacement experiment, fluorescence anisotropy was used to monitor the fraction of RevFI bound to the RRE66 (10 nM of each).

**Table 4.5:** Approximate  $K_d$  values ( $\mu\text{M}$ )\* of  $\Lambda$ -[Ru(bpy)<sub>2</sub>eilatIn]<sup>2+</sup> (**9**),  $\Delta$ [Ru(bpy)<sub>2</sub>eilatIn]<sup>2+</sup> (**10**), ethidium bromide (**12**), and eilatIn (**14**) as calculated from  $C_{50}$  values (Table 4.3).\*

Nucleic Acid	$\Lambda$ -[Ru(bpy) <sub>2</sub> eilatIn] <sup>2+</sup> ( <b>9</b> )	$\Delta$ -[Ru(bpy) <sub>2</sub> eilatIn] <sup>2+</sup> ( <b>10</b> )	ethidium bromide ( <b>12</b> )	eilatIn ( <b>14</b> )
C.T. DNA	5	9.5	2.7	1.5
Poly d(A) – Poly d(T)	2.5	7.5	31	0.5
Poly d(AT) – Poly d(AT)	0.5	< 0.5	0.33	2.5
Poly d(G) – Poly d(C)	3.5	2.5	3.3	2.5
Poly d(GC) – Poly d(GC)	5	24	1.3	4
Poly r(A) – Poly r(U)	2.5	7	2	6
Poly r(G) – Poly r(C)	59	39	130	10
Poly r(I) – Poly r(C)	96	86	53	75
Poly r(U)	< 0.5	< 0.5	1,300	> 1,000
Poly r(C)	22	34	2,700	> 500
Poly r(A)	3	2.5	500	35
Poly r(G)	5	6	76	2
Poly r(I)	2.5	1	310	0.1
Oligo r(I) <sub>15</sub>	30	23	n.d.	n.d.
Poly d(A)	6	96	n.d.	n.d.
Oligo d(A) <sub>15</sub>	96	31	n.d.	n.d.
Oligo d(T) <sub>15</sub>	6.5	6.5	n.d.	n.d.

\* The  $K_d$  values for **14** are estimated to =  $((C_{50} / 2) - 0.05)$ . Consistent with earlier studies, the  $K_d$  values for **12** are  $(K_d \cong ((C_{50} / 3) - 4))$ .<sup>87</sup> For **9** and **10**, the  $K_d$  values are approximately  $\cong ((C_{50} / 2) - 4)$ . These values serve as estimates only, as differences in binding stoichiometries and cooperativity will affect the calculated  $K_d$  values.

Tables 4.4 and 4.5 represent, to the best of our knowledge, the most comprehensive study of ethidium bromide and its affinity to different nucleic acids to date. Bresloff and Crothers used equilibrium dialysis to study the binding of ethidium to 12 different nucleic acids, five of which appear in Table 4.5.<sup>87</sup> These studies were conducted at 1M NaNO<sub>3</sub>, and our studies are conducted at physiological ionic strength (see section E 4.0.2 for experimental conditions). Despite the different conditions, we report similar trends in ethidium affinity for all five nucleic acids.<sup>87</sup>

Tables 4.4 and 4.5 highlight how the nucleic acid specificity of an intercalating ligand can change upon incorporation into an octahedral metal complex. For most, but not all *duplex* nucleic acids, free eilatin (**14**) has a slightly higher DNA and RNA affinity compared to **9** and **10** (Table 4.5). A notable exception is poly d(AT) – poly d(AT). The eilatin-containing metal complexes (**9** and **10**) have a much higher affinity for poly d(AT) – poly d(AT) as compared to poly d(A) – poly d(T), while eilatin (**14**) has the opposite selectivity (Table 4.5).

The trends observed for single-stranded versus double-stranded nucleic acids are strikingly different for **9**, **10**, **11**, and **14** (Table 4.5). Ethidium (**12**) is a “classic” intercalating agent and, hence, has a low affinity for all the single-stranded nucleic acids evaluated (Table 4.5). Molecules with extended aromatic surfaces can, however, show appreciable affinity for single-stranded nucleic acids.<sup>121,122</sup> Both eilatin (**14**) and the eilatin metal complexes bind to single-

stranded nucleic acids, but with very different trends in affinity. Eilatin (**14**) exhibits a high degree of differentiation among the three homopurine single-stranded nucleic acids (poly r(I) > poly r(G) > poly r(A)). This suggests a preference for electron-poor purines. Both eilatin (**14**) and ethidium (**12**) have a much lower affinity for the homopyrimidines (poly r(U) and poly r(C)) as compared to the homopurines (poly r(I), poly r(G), poly r(A)). In contrast, no clear preference of purines versus pyrimidines is seen for **9** and **10** (Table 4.5).

The eilatin metal complexes (**9** and **10**) have, in general, a much higher affinity to single-stranded nucleic acids as compared to both eilatin (**14**) and ethidium (**12**). Compounds **9** and **10** bind to poly r(U) with sub- $\mu$ M affinities. Only one other small molecule, to our knowledge, has been reported to possess high affinity for poly r(U).<sup>121</sup> Given the preferential binding of **9** and **10** to single-stranded nucleic acids, we examined the possibility that the eilatin-containing metal complexes recognize the internal bulge of the RRE (Figure 2.4). This bulge is known to possess single-stranded characteristics in the absence of Rev binding.<sup>123</sup> We have conducted titrations using an inosine-substituted RRE JW (Figure 2.5). This mutant RRE binds to the RevFI peptide with the approximately same affinity (2 nM), but it has over a 2-fold higher affinity for **9** as compared to the RRE JW. This is consistent with these metal complexes exhibiting a higher affinity for single-stranded r(I) versus r(G) (Table 4.5), and suggests that the internal bulge of the RRE is the preferred binding site of these complexes.

To the best of our knowledge, only one other group has examined the nucleic acid affinity of eilatin (**14**), and they reported very different results as compared to ours.<sup>104</sup> Ethidium bromide displacement experiments were conducted using CT DNA, but only a low DNA affinity was suggested ( $IC_{50} > 100 \mu\text{M}$ ).<sup>104</sup> The limited solubility of eilatin (solubility in water  $< 3 \mu\text{M}$ ) may explain this result. The same report also used fluorescence experiments to monitor the change in “emission” of a solution of **14** as a function of CT DNA concentration.<sup>104</sup> They showed an *increase* in the fluorescence intensity of eilatin upon addition of CT DNA. We find a decrease for all nucleic acids tested (Figure 4.10). In their case, however, the sample was both excited and monitored at 520 nm.<sup>104</sup> Eilatin shows no absorption at this wavelength.<sup>101</sup> Since the sample was excited and monitored at the *same* wavelength, the increase in “emission” was actually the increased light scattering by the solution upon titration of DNA.<sup>104</sup>

Eilatin-containing metal complexes are new anti-HIV agents with unusual nucleic acid specificities. The eilatin ligand is essential for nucleic acid binding and the anti-HIV activity of these compounds, but the free ligand exhibits drastically different trends in nucleic acid affinity as compared to the eilatin-containing metal complexes. Unusual trends in enantiomeric selectivity, single-stranded nucleic acid binding, and sequence specificity make the eilatin-containing metal complexes two of the most unusual, and best characterized, RRE ligands to date.